Electronic supplementary information

Integrating Z-scheme heterojunction of Co_1-C_3N_4@α-Fe_2O_3 for efficient visible-light-driven photocatalytic CO_2 reduction

Bing-Cai He, Chao Zhang, Pei-Pei Luo, Yu Li* and Tong-Bu Lu*

MOE International Joint Laboratory of Materials Microstructure, Institute for New Energy Materials and Low Carbon Technologies, School of Materials Science & Engineering, Tianjin University of Technology, Tianjin 300384, China.

*Corresponding authors: Yu Li (yli@email.tjut.edu.cn); Tong-Bu Lu (lutongbu@tjut.edu.cn)

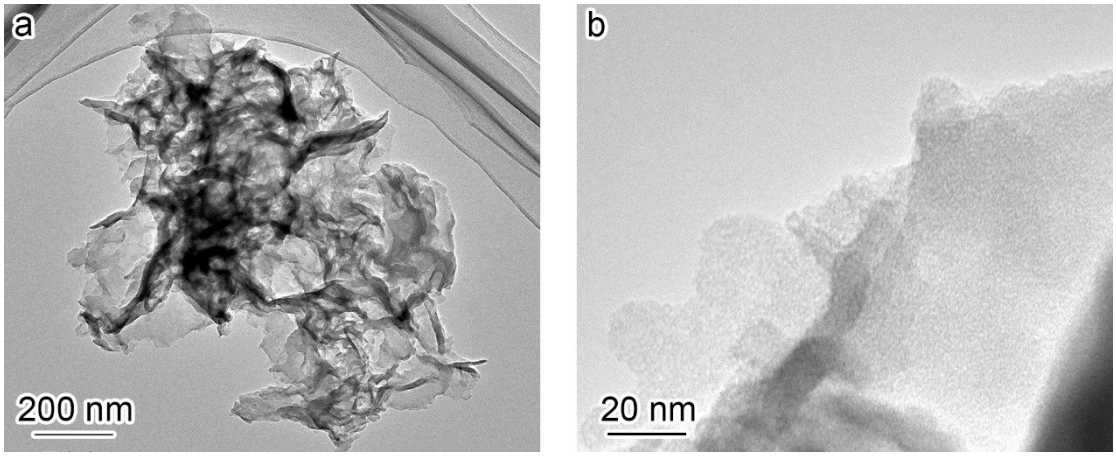

Figure S1. TEM images for Co_1-C_3N_4.

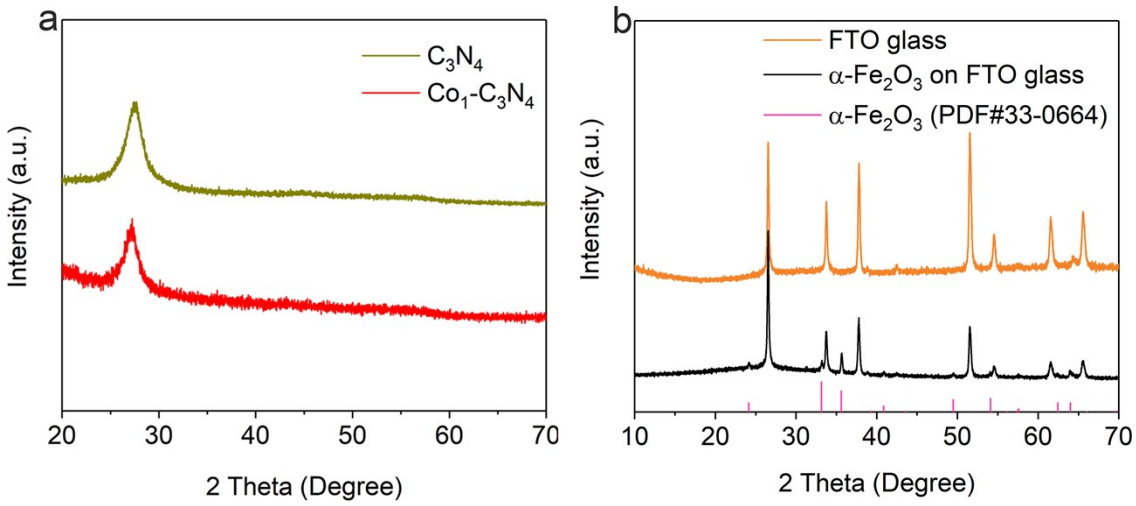

Figure S2. XRD patterns for (a) g-C_3N_4, Co_1-C_3N_4 and (b) α-Fe_2O_3.

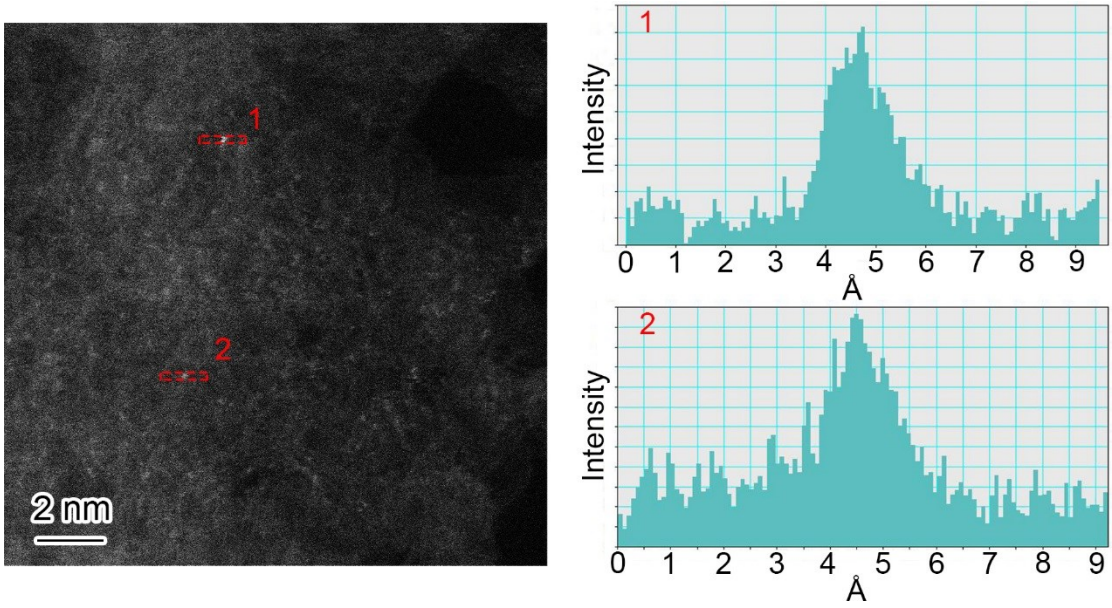

Figure S3. Atomic-resolution HAADF-STEM image for Co_1-C_3N_4@α-Fe_2O_3 and the corresponding intensity profiles for region 1 and 2.

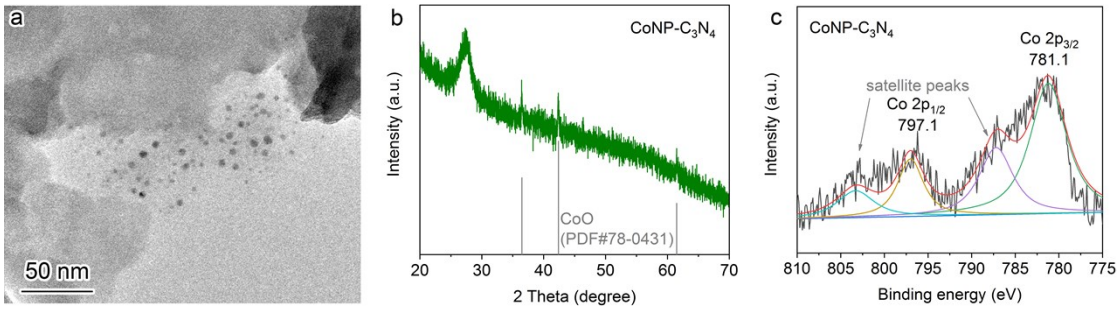

Figure S4. (a) TEM image, (b) XRD pattern and (c) Co 2p XPS spectrum for CoNP-C_3N_4.

As shown in Figure S4b, the Co nanoparticles in CoNP-C_3N_4 were determined to be CoO. Moreover, as revealed in Figure S4c, the strong satellite peaks and the binding energies of Co $2p_{3/2}$ and Co $2p_{1/2}$ further validate the Co(II) state of the Co species in CoNP-C_3N_4, which is consistent with the valence state of the single-atomic Co sites in Co_1-C_3N_4 (Fig. 4d & Table S3).[1]

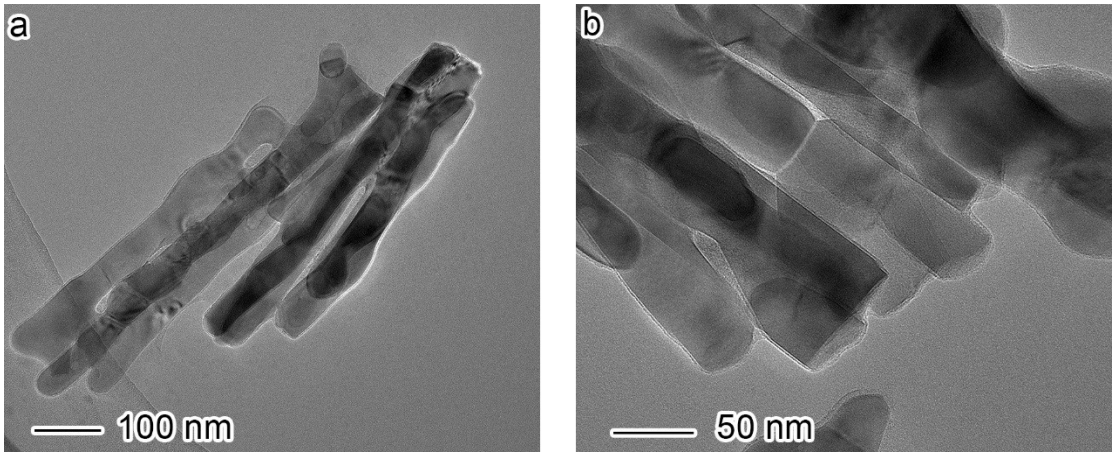

Figure S5. TEM images for α-Fe_2O_3 nanorods.

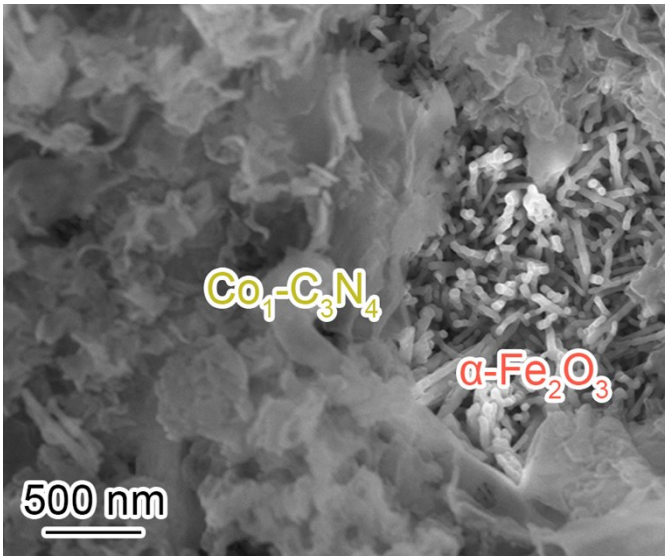

Figure S6. SEM image for Co_1-C_3N_4@α-Fe_2O_3.

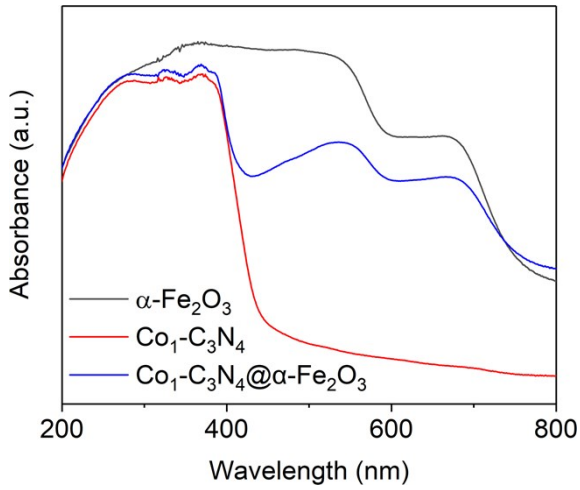

Figure S7. UV–vis diffuse reflectance spectra for α-Fe_2O_3, Co_1-C_3N_4, and Co_1-C_3N_4@α-Fe_2O_3.

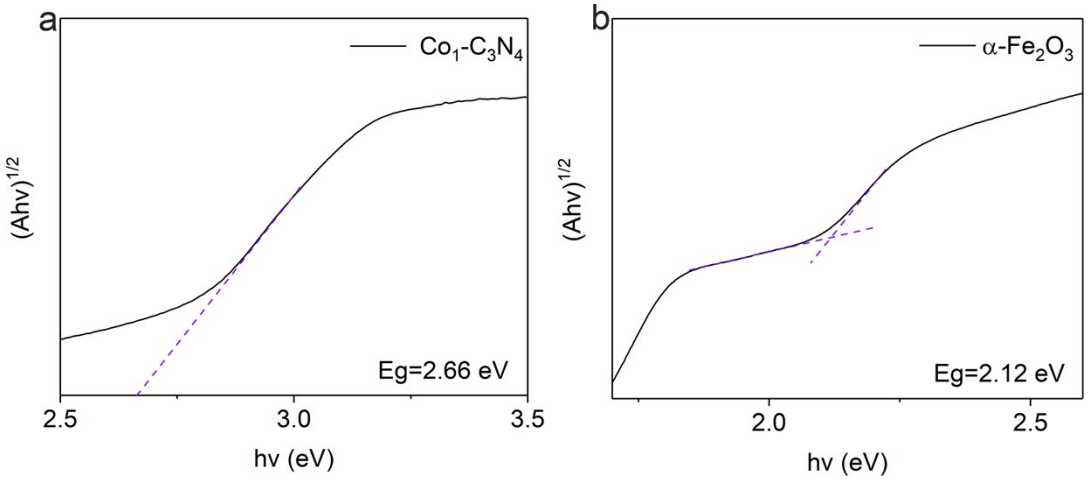

Figure S8. Calculated bandgaps for (a) Co_1-C_3N_4 and (b) α-Fe_2O_3.

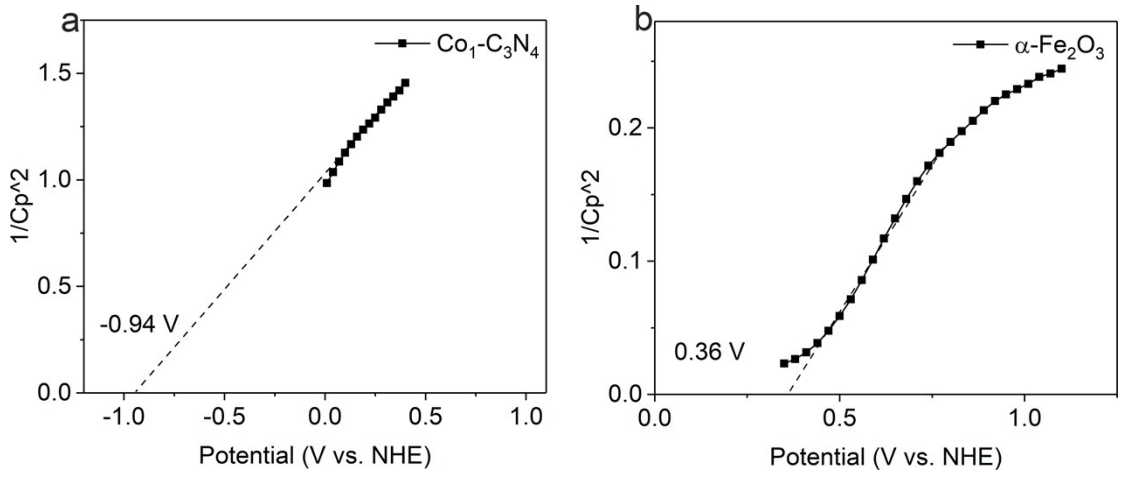

Figure S9. Mott–Schottky plots for (a) Co_1-C_3N_4 and (b) α-Fe_2O_3.

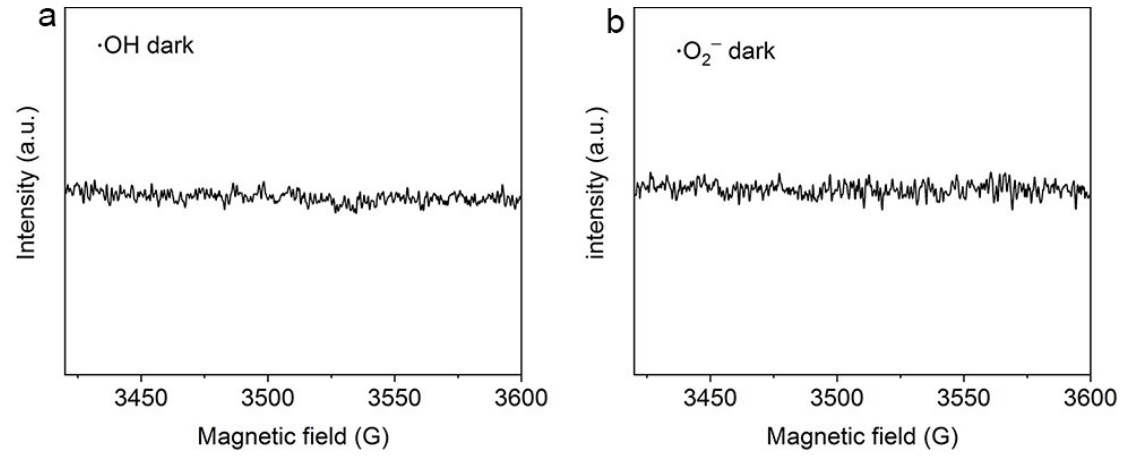

Figure S10. DMPO spin-trapping ESR spectra for Co_1-C_3N_4@α-Fe_2O_3 under dark condition.

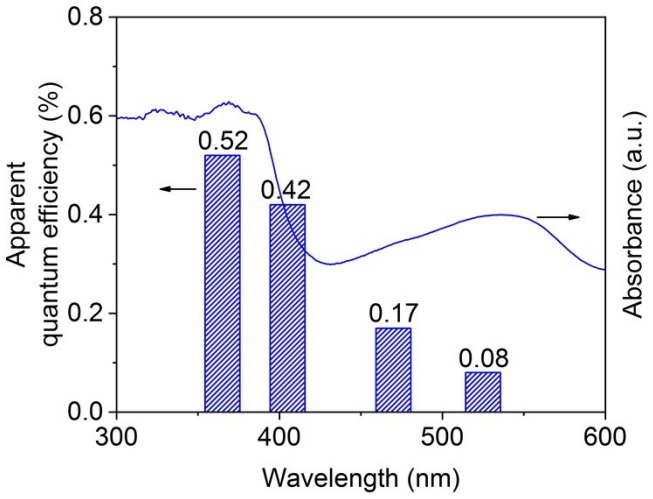

Figure S11. Apparent quantum efficiencies of Co_1-C_3N_4@α-Fe_2O_3.

Apparent quantum efficiencies (AQEs) for CO generation was tested under different wavelengths (365 nm, 405 nm, 470 nm, and 525 nm) with a fixed power density of 10 mW cm^{-2}, and calculated by the equation:

$$AQE = \frac{2 \times n(CO) \times N_A}{t \times P \times S/E_{photon}} \times 100\%$$

where n(CO) is the amount of CO generation, N_A is the Avogadro constant, t is the reaction time, P is the power density of the incident light, S is the irradiated area, and E_{photon} is the energy of the photon of the incident light.

It can be clearly observed that the AQEs decrease as the wavelengths of the incident light increase, indicating that the CO generation strongly depends on the wavelength of the incident light.

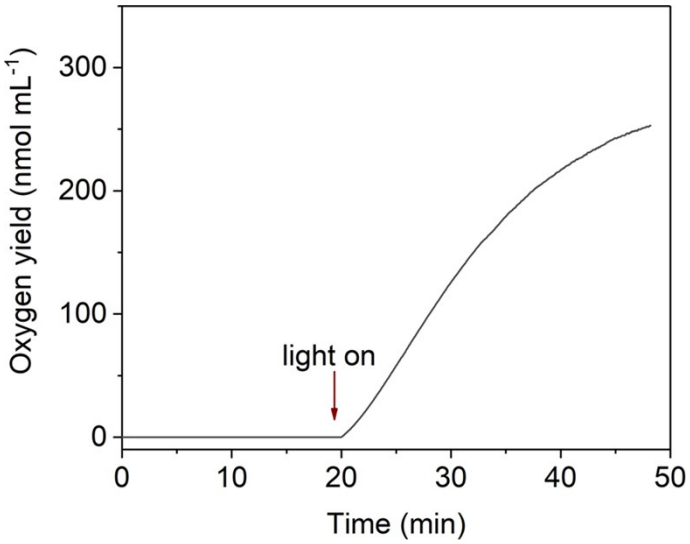

Figure S12. Time profiles of oxygen yield for Co_1-C_3N_4@α-Fe_2O_3 under visible-light irradiation.

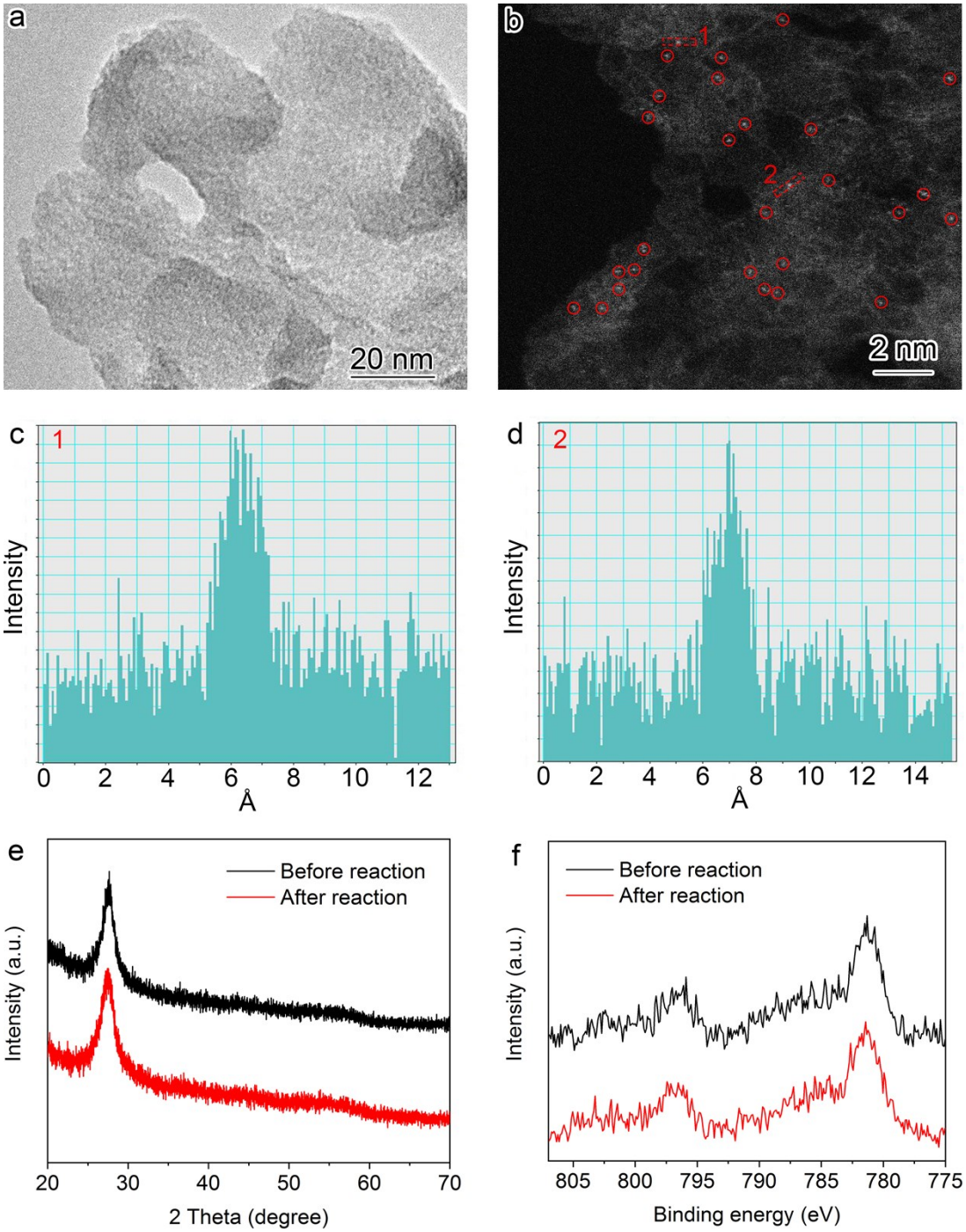

Figure S13. (a) TEM image, (b) atomic-resolution HAADF STEM image, and (e) XRD pattern for Co_1-C_3N_4 carefully scraped from Co_1-C_3N_4@α-Fe_2O_3 after six consecutive cycles of photocatalytic CO_2 reduction reaction. (C, D) Corresponding intensity profiles for region 1 and 2 in (b). (f) Co 2p XPS spectra for Co_1-C_3N_4@α-Fe_2O_3 before and after the stability test.

As revealed by Figure S13a and b, the atomic dispersion of the Co sites was well

maintained, and no aggregation was observed after the six consecutive cycles of photocatalytic CO_2 reduction reaction. In addition, XPS measurements (Figure S13f) showed that after the photocatalytic reduction of CO_2, the single-atomic Co sites remained their Co(II) state. These results strongly confirm the stability of the Co_1-C_3N_4@α-Fe_2O_3.

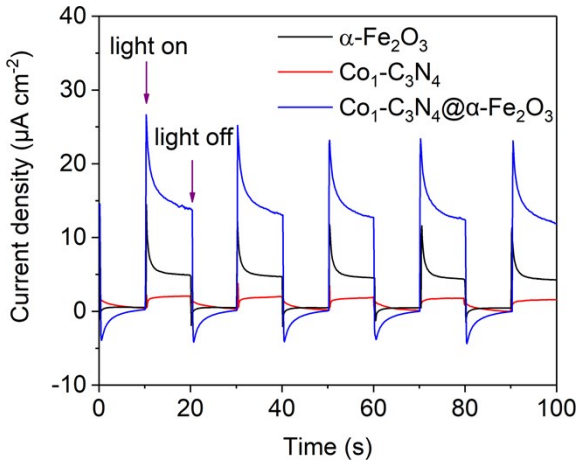

Figure S14. Transient photocurrent response under visible-light irradiation for α-Fe_2O_3, Co_1-C_3N_4, and Co_1-C_3N_4@α-Fe_2O_3.

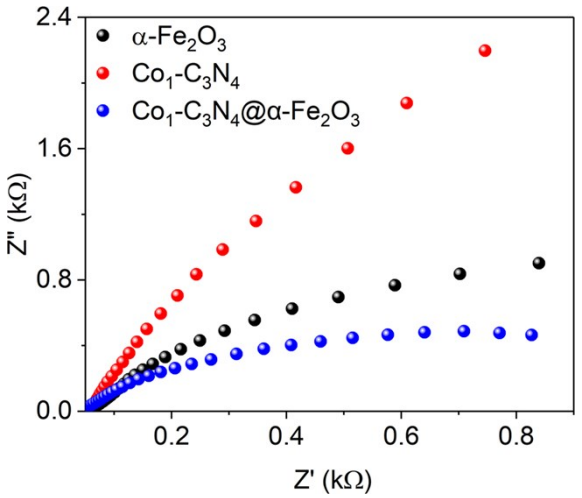

Figure S15. EIS Nyquist plots for α-Fe_2O_3, Co_1-C_3N_4, and Co_1-C_3N_4@α-Fe_2O_3 under visible light.

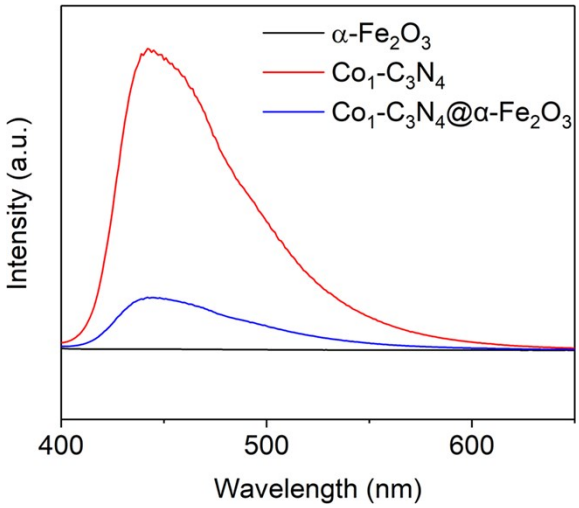

Figure S16. PL spectra for α-Fe_2O_3, Co_1-C_3N_4, and Co_1-C_3N_4@α-Fe_2O_3.

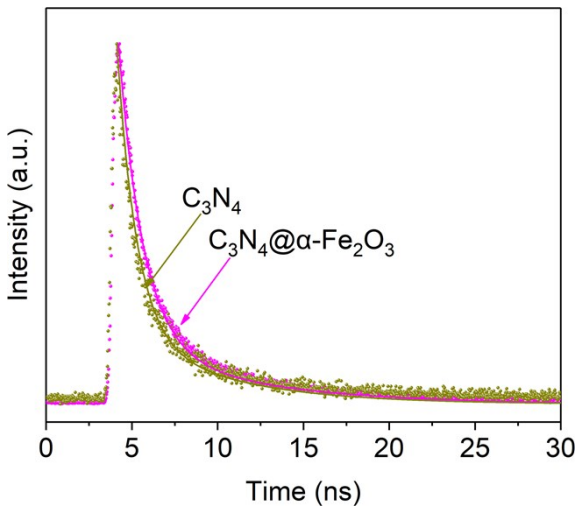

Figure S17. Time-resolved photoluminescence decay curves for g-C_3N_4 and C_3N_4@α-Fe_2O_3.

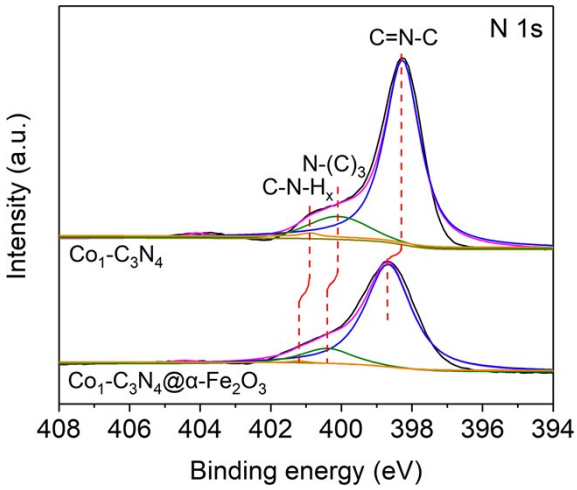

Figure S18. N 1s core-level spectra for Co_1-C_3N_4 and Co_1-C_3N_4@α-Fe_2O_3.

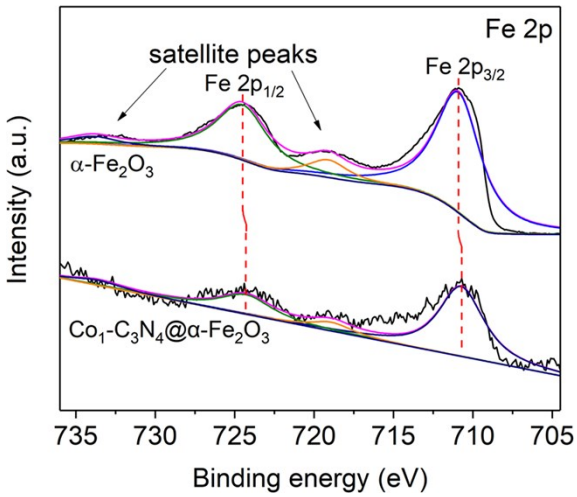

Figure S19. Fe 2p core-level spectra for α-Fe_2O_3 and Co_1-C_3N_4@α-Fe_2O_3.

Table S1. Cobalt contents of Co_1-C_3N_4 and CoNP-C_3N_4, determined by ICP-MS.

Catalyst	Co (wt.%)
Co_1-C_3N_4	0.07
CoNP-C_3N_4	0.81

Table S2. The calculated photoluminescence decay lifetimes.

Sample	τ_1 (ns)	A_1 (%)	τ_2 (ns)	A_2 (%)	τ (ns)
α-Fe_2O_3	0.55	86.44	3.00	13.56	1.70
g-C_3N_4	1.13	79.31	5.90	20.69	3.89
Co_1-C_3N_4	1.50	83.22	7.40	16.78	4.44
C_3N_4@α-Fe_2O_3	1.41	82.48	7.23	17.52	4.45
Co_1-C_3N_4@α-Fe_2O_3	1.52	74.86	7.40	25.14	5.17

The average luminescence lifetimes (τ), the calculated photoluminescence decay lifetimes (τ_1 and τ_2) and the magnitude factors (A_1 and A_2) were determined from a double-exponential fitting of the decay curves. The average luminescence lifetime (τ) was calculated according to the equation:

$$\tau = \frac{A_1{\tau_1}^2 + A_2{\tau_2}^2}{A_1\tau_1 + A_2\tau_2}$$

Table S3. The binding energies of N 1s and Co 2p.

Sample	N 1s Binding energy (eV)			Co 2p Binding energy (eV)	
	C=N-C	$N-(C)_3$	$C-N-H_X$	$2p_{1/2}$	$2p_{3/2}$
$Co_1-C_3N_4$	398.3	400.1	400.9	796.4	781.1
$Co_1-C_3N_4$@α-Fe_2O_3	398.7	400.4	401.2	796.7	781.4

Table S4. The binding energies of Fe 2p.

Sample	Fe 2p Binding energy (eV)	
	$2p_{1/2}$	$2p_{3/2}$
α-Fe_2O_3	724.5	710.9
$Co_1-C_3N_4$@α-Fe_2O_3	724.3	710.7

Table S5. Comparison of the performance with those reported catalysts for photocatalytic CO_2 reduction.

Photocatalyst	Light source	Reaction medium	Product	Photocatalytic activity ($\mu mol\ g^{-1}\ h^{-1}$)	Selectivity (%)	Ref.
Co_1-C_3N_4@α-Fe_2O_3	300 W Xe lamp full spectrum	Gas–solid, H_2O	CO	25.2	> 99	This work
Co_1-C_3N_4@α-Fe_2O_3	300 W Xe lamp $\lambda > 400$ nm	Gas–solid, H_2O	CO	14.9	> 99	This work
□α-Fe_2O_3/g-C_3N_4	300 W Xe lamp full spectrum	Gas–solid, H_2O	CO	27.2	> 99	2
Co^{2+}@C_3N_4	Halogen lamp $\lambda > 420$ nm	Liquid-solid MeCN/TEOA	CO	25.5	> 99	3
Er_1/CN-NT	300 W Xe lamp $\lambda > 420$ nm	Liquid-solid H_2O	CH_4 CO	2.5 47.1	17.5 82.5	4
Au_1@C_3N_4	300 W Xe lamp $\lambda > 420$ nm	Gas–solid, H_2O	CH_4 CO	1.0 8.7	31.5 68.5	5
a-Mo_1/C_3N_4	300 W Xe lamp $\lambda > 420$ nm	Gas–solid, H_2O	CO H_2	18.0 37.0	32.7 67.3	6
Cu_1-CCN	300 W Xe lamp full spectrum	Gas–solid, H_2O	CH_4 CO	0.05 3.1	6.1 93.9	7
CN-ATZ-NaK	350 W Xe lamp full spectrum	Gas–solid, H_2O	CH_4 CO CH_3OH	14.1 1.1 0.5	97.2 1.9 0.9	8
BIF-20@g-C_3N_4	300 W Xe lamp $\lambda > 400$ nm	Liquid-solid MeCN/TEOA	CH_4 CO	15.5 53.9	53.5 46.5	9
Co_1-Bi_3O_4Br-1	300 W Xe lamp full spectrum	Liquid-solid H_2O	CO	107.1	> 99	10
Cu_1-mTiO_2	300 W Xe lamp full spectrum	Gas–solid, H_2O	CH_4 CO H_2	4.6 0.9 0.8	91.5 4.5 4.0	11

(*Continued*)

Cu_1-TiO_2 nanosheet	300 W Xe lamp full spectrum	Liquid-solid H_2O	CO	1.6	> 99	12
Co tuned Au nanocluster	300 W Xe lamp λ > 420 nm	Liquid-solid H_2O/TEOA	CH_4 CO H_2	0.08 3.5 1.5	6.0 65.8 28.2	13
Ni doped CdS quantum dot	300 W Xe lamp λ > 400 nm	Liquid-solidH_2O/TEOA	CH_4 CO	1.1 9.5	31.7 68.3	14
BON-Br	300 W Xe lamp full spectrum	Gas–solid, H_2O	CO	8.1	> 99	15

References

1. B. J. Tan, K. J. Klabunde and P. M. A. Sherwood, J. Am. Chem. Soc., 1991, 113, 855-861.
2. Z. Jiang, W. Wan, H. Li, S. Yuan, H. Zhao and P. K. Wong, *Adv. Mater.*, 2018, **30**, 1706108.
3. P. Huang, J. Huang, S. A. Pantovich, A. D. Carl, T. G. Fenton, C. A. Caputo, R. L. Grimm, A. I. Frenkel and G. Li, *J. Am. Chem. Soc.*, 2018, **140**, 16042-16047.
4. S. Ji, Y. Qu, T. Wang, Y. Chen, G. Wang, X. Li, J. Dong, Q. Chen, W. Zhang, Z. Zhang, S. Liang, R. Yu, Y. Wang, D. Wang and Y. Li, *Angew. Chem. Int. Ed.*, 2020, **59**, 10651-10657.
5. Y. Yang, F. Li, J. Chen, J. Fan and Q. Xiang, *ChemSusChem*, 2020, **13**, 1979-1985.
6. R. Zhang, P. Li, F. Wang, L. Ye, A. Gaur, Z. Huang, Z. Zhao, Y. Bai and Y. Zhou, *Appl. Catal., B*, 2019, **250**, 273-279.
7. Y. Li, B. Li, D. Zhang, L. Cheng and Q. Xiang, *ACS Nano*, 2020, DOI: 10.1021/acsnano.0c04544.
8. G. Zhang, G. Li, T. Heil, S. Zafeiratos, F. Lai, A. Savateev, M. Antonietti and X. Wang, *Angew. Chem. Int. Ed.*, 2019, **58**, 3433-3437.
9. G. Xu, H. Zhang, J. Wei, H.-X. Zhang, X. Wu, Y. Li, C. Li, J. Zhang and J.

Ye, *ACS Nano*, 2018, **12**, 5333-5340.

10. J. Di, C. Chen, S.-Z. Yang, S. Chen, M. Duan, J. Xiong, C. Zhu, R. Long, W. Hao, Z. Chi, H. Chen, Y.-X. Weng, J. Xia, L. Song, S. Li, H. Li and Z. Liu, *Nat. Commun.*, 2019, **10**, 2840.
11. L. Yuan, S.-F. Hung, Z.-R. Tang, H. M. Chen, Y. Xiong and Y.-J. Xu, *ACS Catal.*, 2019, **9**, 4824-4833.
12. Z. Jiang, W. Sun, W. Miao, Z. Yuan, G. Yang, F. Kong, T. Yan, J. Chen, B. Huang, C. An and G. A. Ozin, *Adv. Sci.*, 2019, **6**, 1900289.
13. X. Cui, J. Wang, B. Liu, S. Ling, R. Long and Y. Xiong, *J. Am. Chem. Soc.*, 2018, **140**, 16514-16520.
14. J. Wang, T. Xia, L. Wang, X. Zheng, Z. Qi, C. Gao, J. Zhu, Z. Li, H. Xu and Y. Xiong, *Angew. Chem. Int. Ed.*, 2018, **57**, 16447-16451.
15. L. Hao, L. Kang, H. Huang, L. Ye, K. Han, S. Yang, H. Yu, M. Batmunkh, Y. Zhang and T. Ma, *Adv. Mater.*, 2019, **31**, 1900546.